ELSEVIER

A Pullout Test for Determining Interface Properties between Rebar and Concrete

W. Yeih, R. Huang, J.J. Chang, and C.C. Yang*
*Department of Harbor and River Engineering, and *Institute of Materials Engineering*
National Taiwan Ocean University, Keelung, Taiwan, R.O.C.

In this study, the rebar-concrete interface properties were investigated by conducting the single rebar pullout test. Using a combination of the stress approach and fracture mechanical theory, the corresponding material parameters were obtained and the model was verified as being suitable for reinforced concrete composite material. ADVANCED CEMENT BASED MATERIALS 1997, 5, 57–65.

KEY WORDS: Concrete, Rebar, Interface, properties, Pullout test, Failure mode

The bond between the rebar and the matrix in a rebar-reinforced brittle matrix material is one of the major factors affecting the mechanical behavior of this composite material. Najm [1] indicated that three forces exist on the rebar-concrete interface: the chemical adhesion between the rebar and concrete, the frictional force between the rebar and concrete, and the interlock force resulting from the ribs of the rebar. Edwards and Yannopulous [2] reported that the ultimate pullout force for smooth steel bars was only 1/3 to 1/2 of that for deformed rebars. It was also reported [3] that bond resistance is mainly provided by the interlock effect. When bond stress is low, the rib will first induce inclined cracks because of the interface effect as shown in Figure 1. After inclined cracks form, the tensile stress of the rebar is transmitted to the concrete through the contact force on the surface of the ribs. The radial component of this contact force is called the splitting pressure, and it may result in splitting failure provided it becomes large enough. However, if the confinement of the concrete is strong enough to prevent splitting failure, the dominant failure mode will be shear pullout failure. The typical load-displacement curve of concrete with and without confinement is also illustrated in Figure 1, and it appears that the confinement effect results in different mechanical behaviors. Ezeldin and Balaguru [4] reported that the failure mode of the pullout test in #3 rebar-concrete composite was shear pullout failure, and that splitting failure occurred in specimens with #5, #6, and #8 rebars. They also found other types of failure, e.g., cone shape tensile failure and splitting-tensile failure, for specimens with larger rebars.

To study the bond behavior between rebar and the concrete interface, beam specimens have frequently been tested [5–7]. Based on the testing results of beam specimens, the development length parameter was derived. Orangun *et al.* [8] proposed an empirical formula in which the development length is expressed as a function of the embedded length of the rebar, the thickness of the concrete cover, the splice space, the diameter of the rebars, the effect of stirrup, and the compressive strength of the concrete. Their findings were later adopted by ACI committee 408. The beam-specimen approach is practical for engineering applications. Because of the complexity of the stress state in a beam specimen, it is very difficult to obtain the material properties of the interface. On the other hand, the single rebar/fiber pullout test may provide some information about interface properties by simplifying the stress state. Therefore, many researchers [9–11] have recently carried out single rebar/fiber pullout tests to analyze bond behavior. In addition, many theories [12–16] can be applied to predict pullout behaviors and to obtain the interface properties. Although application of theoretical models may be somewhat improper for predicting the rebar-concrete interface properties because of the circular cylindrical rebar assumption, it is still an effective way to analyze the bond behavior of the rebar-concrete interface using interface parameters. All the theoretical models are based on several assumptions which need to be verified before application. In Stang's model [14], the Poisson effect is neglected in the interface layer, and the frictional shear force is assumed to be uniformly distributed throughout the debonding zone. Such assumptions might not be appropriate for some composite materials, therefore theoretical models should be verified by experimental data. For example, in Stang's model [14], four material constants were proposed which were independent of the embedded length

ISSN 1065-7355/97/$17.00
PII S1065-7355(96)00004-1

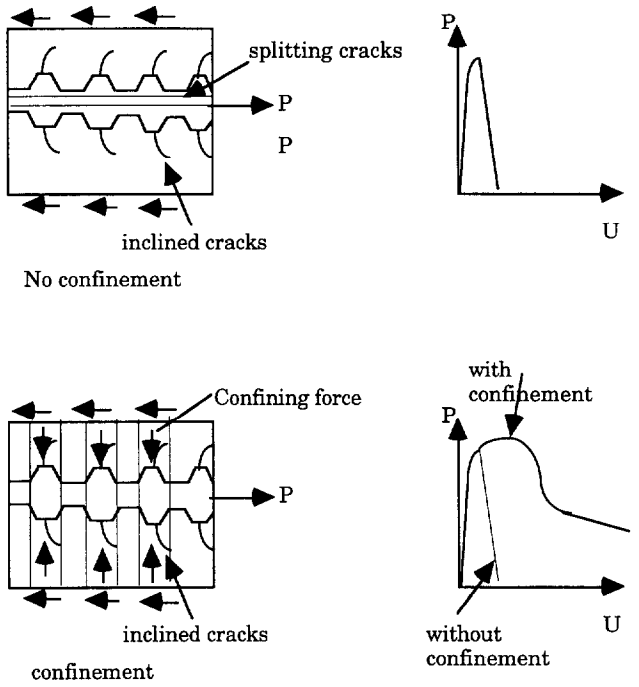

FIGURE 1. Failure types for concrete specimens with and without confinement.

of the rebar/fiber. Therefore, for a specific rebar-matrix combination, the validity of Stang's model can be examined. Another approach to stress analysis of pullout specimens is numerical implementation [17–18].

In this study, Stang's model [14] for rebar-concrete composite material was applied and evaluated based on the material properties. The material constants were obtained from experimental results.

Theoretical Background

Stang *et al.* [14] developed a theoretical model which was based on a single fiber with a length of L (in this study, rebar is considered as a fiber) embedded in a matrix as shown in Figure 2. Their theory assumes that the fiber/rebar has a constant cross-sectional area, A, and a Young's modulus, E_f. In the model, the pullout force reacts against the remote stress from concrete at infinity, which is quite different from the experimental condition where pullout force is balanced by the compressive forces on concrete in the vicinity of the rebar. Because the model assumes concrete (except that in the matrix shear lag) as a rigid support, it does not matter where the reaction forces are located because of the transmissibility of forces through the rigid body.

The rebar displacement, U, and axial load, P, over the rebar cross section can be expressed as

$$P = E_f A U', \tag{1}$$

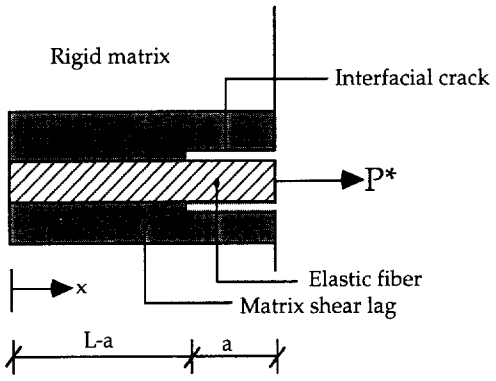

FIGURE 2. Mathematical model used in Stang's model.

where the derivative with respect to x is denoted by ', and U is the rebar displacement in the longitudinal direction.

Introducing the shear force per unit length, q, acting on the interface, the equilibrium equation for the rebar can be written as

$$P' - q = 0. \tag{2}$$

The matrix is modeled as a shear lag with shear stiffness k on a rigid support. The relationship between the shear force per length acting at the interface and the displacement in the shear lag at the interface is given by

$$q = kU \tag{3}$$

in the perfect bonded zone.

The effect of Poisson's ratio is neglected in both the rebar and boundary layer so the model is a one-dimensional mathematic problem. Therefore it becomes impossible to represent the splitting pressure in their model, and splitting failure is not taken into account. If the failure of specimens is dominated by the shear pullout failure, then the confinement of the concrete is assumed to be strong enough to prevent splitting failure so that only longitudinal behavior is considered.

It is assumed that debonding has occurred over a given length, a, starting at $x = L$, then the interfacial conditions can be written as

$$U \text{ (in the matrix)} = U \text{ (in the fiber)}, \quad 0 \leq x \leq L - a, \tag{4a}$$

$$q = q^*, \quad L - a < x \leq L, \tag{4b}$$

where q^* is the constant frictional shear force per length in the debonding zone. Applying boundary conditions at $x = 0$ and $x = L$ and continuity conditions at $x = L - a$, the fiber displacement U^* at $x = L$ can be written as

$$U^* = U(x = L) = \frac{P^* - q^*a}{E_f A \varpi}\coth[\varpi(L-a)] + \frac{P^* - \frac{1}{2}q^*a}{E_f A}a, \tag{5}$$

where P^* is the axial load at x = L and $\varpi = \sqrt{k/E_f A}$.

In a previous study by Stang *et al.*, two approaches were used to describe the debonding behavior. The first approach was based on the stress criterion which assumes debonding occurs when the shear force per length reaches a critical value, q_y, at crack tip x = $L - a$. In addition, the shear force per length in the debonding zone is assumed to be

$$q^* = Dq_y,\ 0 \leq D \leq 1. \tag{6}$$

D is a parameter which represents the remaining shear effect, including the frictional and interlock force in the debonding. Thus, the following formula is derived:

$$P^* = q^*a + \frac{q_y}{\varpi}\tanh[\varpi(L-a)]. \tag{7}$$

Using eq 7 and letting $a = 0$, P_y^* is obtained as

$$P_y^* = q_y\frac{\tanh(\varpi L)}{\varpi}, \tag{8}$$

where P_y^* is the axial yielding load at x = L while debonding only occurs at x = L.

The second approach was based on the energy criterion which is based on the fracture mechanical theory. The displacement continuity assumption is applied assuming that the displacement in the matrix shear lag along the debonded interface is constant and equal to $U(L - a)$, as an approximation for the shear lag strain energy and work done by the frictional force. Using this assumption, the axial load at x = L can be expressed as

$$P_{(U)}^* = q^*a + \left[\frac{q^*}{2\varpi} + \sqrt{\left(\frac{q^*}{2\varpi}\right)^2 + 2E_f Ap\Gamma}\right]\tanh[\varpi(L-a)], \tag{9}$$

where p is the perimeter of the fiber, and Γ is the surface energy.

Another assumption is that the shear force per length along the debonded interface is equal to q^*, and that the displacement in the shear lag along the interface is given by the constitutive relation, eq 3. The axial load at x = L can then be written as

$$P_{(q)}^* = q^*a + \left(\frac{q^*}{\varpi} + \sqrt{2E_f Ap\Gamma}\right)\tanh[\varpi(L-a)]. \tag{10}$$

By arranging eq. 7, eq. 9 and eq. 10, the relationship between D and Γ can be written as

$$D_{(U)} = \left[\frac{1}{2} + \sqrt{\left(\frac{1}{2}\right)^2 + \frac{2kp\Gamma}{(q^*)^2}}\right]^{-1}, \tag{11a}$$

$$D_{(q)} = \left[1 + \sqrt{\frac{2kp\Gamma}{(q^*)^2}}\right]^{-1}. \tag{11b}$$

By examining eqs. 11a and 11b, D is found to always be less than 1. However, the confining forces might induce interface hardening so that the shear force per length becomes larger after debonding, i.e., $D > 1$. In this case, the shear strain in the shear lag and the work done by the frictional force cannot be calculated using the above model. Thus, the constitutive relationship between the shear force and the longitudinal displacement of the rebar can be modified as a constitutive relationship between the shear force per length in the shear lag and the displacement jump on the interface, i.e., the difference of the longitudinal displacements between the rebar and nearby concrete (matrix shear lag). Assuming linear hardening behavior in the interface after debonding, the above-mentioned relationship can be written as $q = q_y + T(U_{fiber} - U_{interface})$, where T is the bond modulus [9] representing the linear hardening behavior after debonding. However, the longitudinal displacement relationship between the rebar and concrete at the interface relies on the Poisson effect for both the concrete and rebar, and this is not included in the Stang's model. Based on this fact, another model was proposed [9]. In our study, Stang's model was applied to predict the behavior of the concrete-rebar interface, and experimental data showed that the model was still adequate. This means that the confinement is large enough to prevent splitting pressure and that the remaining shear force per length is not greater than the critical value. The displacement continuity approach was selected because the surface energy obtained by using this approach or by other methods was almost the same.

In this investigation, bond failure was the dominant failure mode, however split failure or rebar yielding could occur. Therefore, application of the model is limited to bond failure conditions.

Analytical Procedures

A typical pullout load-displacement curve is shown in Figure 3. From the curve, a linear relationship exists

Advn Cem Bas Mat
1997;5:57–65

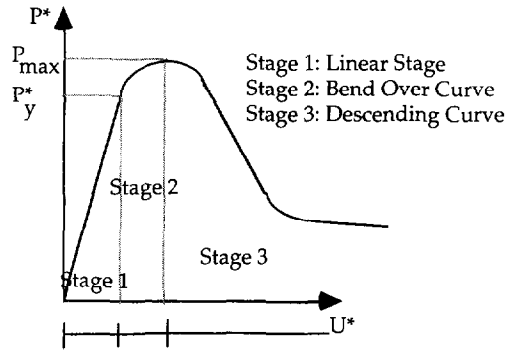

FIGURE 3. Typical load-displacement curve.

between the load and displacement in the first stage. In this stage, it seems that no debonding occurs, i.e., $a = 0$. Based on the slope of the $P^* - U^*$ curve, ϖ and k can be obtained from eq. 5. After k is obtained, the slope of the $P^* - U^*$ curve, λ, in the first stage can be obtained by substituting $a = 0$ and k into eq. 5.

After first stage, the load-displacement curve becomes nonlinear and reaches the second stage. The loading, P_y^*, at the turning point is defined, and interface debonding begins. q_y can then be determined from eq. 8. On the pullout force vs. displacement curve, the turning point, P_y^*, may not be clearly determined. By subtracting λU^* from the loading, P^*, U_y which is the displacement corresponding to the turning point load P_y, can then be determined by using the intersection point of $P^* - \lambda U^*$ vs. U^* curve and the U^* axis. The yielding load, P_y^*, is then calculated from $P_y^* = \lambda U_y$. P_y^* may be perturbed a little bit by the λ value (equivalently the k value), which is dependent on the selected data for the linear regression in the first stage and on the error in the measurements. The allowable error of P_y^* is within 100 N, so that no significant inaccuracy exists in the other parameters resulting from P_y.

At the extreme value of P^*, the slope of the $P^* - U^*$ curve reaches zero, i.e. $dP^*/dU^* = 0$. By using the chain rule, $dP^*/dU^* = (dP^*/da)(da/dU^*) = 0$, it appears that $dP^*/da = 0$ provided that $da/dU^* \neq 0$. By taking the derivative of eq. 9 (or eq. 10) with respect to the interfacial crack length a and setting to zero, solve it with eq. 11a (or eq. 11b provided the derivative of eq. 10 is used) and eq. 5 simultaneously, D, Γ and the debonding length at the maximum load $a_{P_{max}}$ can be obtained. It seems that D and Γ can be obtained by using the data of two points, i.e., the point corresponding to the yielding load P_y^*, and another point corresponding to the maximal load P_{max}, however, the curve between these two data points in the second stage can be determined by using two parameters, D and Γ (eq. 9 for load, eq. 5 for displacement, and a is between zero and $a_{P_{max}}$). If these two data points on the curve are known, the two unknown parameters can be obtained. Using the experimental data in this stage, the optimal D and Γ can be found by employing the least square error method (by fitting eq. 9, 11a and 5 optimally). In this study, the least square method was also applied to obtain the parameters, and no significant difference was found between the two approaches.

In the third stage the descending curve occurs after passing the maximum load. The interface failure propagates further after the maximum load and the entire rebar slips after complete debonding. The contact surface area between the rebar and the matrix becomes smaller as the slip displacement becomes larger. The concrete by the rebar also becomes smooth, which reduces the interlock resistance force. This changes the trend in the load-displacement curve. However, Stang's model did not take the descending behavior into account.

From the above-mentioned procedures, four material parameters, k, q_y, D and Γ, can be found and are independent of the embedded length provided that Stang's model is valid. In the theoretical model, the rebar is assumed to be cylindrical; although the effect of the ribs of the rebar can be implicitly included in the material parameters by considering the rebar to be a cylindrical fiber.

Experimental Details

Specimen

MATERIALS. Type I Portland cement conforming to ASTM 150 was used. Sand and crushed stone were from local sources. The concrete mix design is listed in Table 1. The reinforcing steel was made of medium carbon steel with a Young's modulus of 203 GPa (29435 ksi) and a yield strength of 410 MPa (59.5 ksi). Two nominal diametrical rebars, 0.95 cm (⅜ in) and 1.27 cm (½ in), were used, and the details of rebar geometry are given in Table 2.

SPECIMEN PREPARATION. The specimens were cast in a ϕ10 cm × 20 cm (ϕ4 in × 8 in) steel mold with reinforcing steel positioned at the center. To ensure that the rebar was in a straight vertical position, an accessory device was designed. After demolding, the specimens were

TABLE 1. Mix design for concrete (W/C = 0.583)

Materials	Mix proportions, Kg/m^3 (slug/ft^3)
Water	204 (0.396)
Cement	350 (0.680)
Sand	745 (1.448)
Aggregate	1024 (1.990)

TABLE 2. Details of the rebar geometry

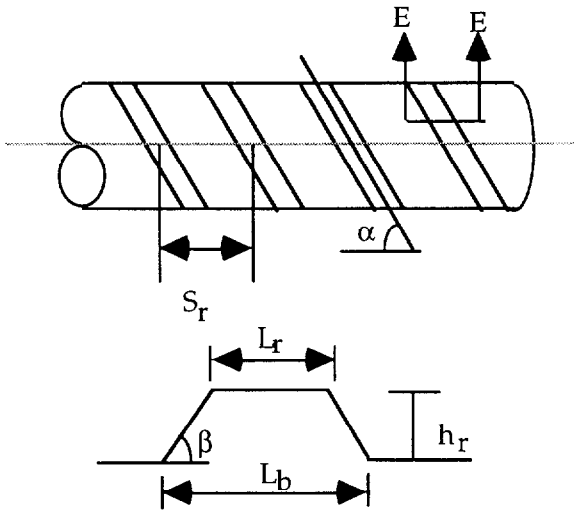

E-E cross section

Number of steel rebars	d_n, Nominal diameter, cm (in)	Nominal area, cm^2 (in^2)	α deg	β deg	S_r mm (in)	L_r mm (in)	h_r mm (in)	L_b mm (in)
3	0.9525 (0.375)	0.7125 (0.1104)	65	53.1	5.92 (.233)	1.33 (.052)	0.52 (.020)	2.11 (.083)
4	1.27 (0.5)	1.2668 (0.1964)	65	53.7	7.84 (.309)	1.81 (.071)	0.84 (.033)	3.05 (.120)

cured for 56 days. The compressive strength of the concrete at 56 days was 35.9 MPa (5,200 psi). The specimen surface for the single-fiber pullout test was capped before the loading test was performed.

VARIABLES CONSIDERED. In order to find the material parameters of the rebar-concrete interface and to verify Stang's model, it was necessary to change the embedded length of rebars. In Stang's model, however, the bond failure is the dominant mode, and the embedded lengths of the rebar are selected to prevent other types of failure such as splitting failure of concrete and yielding of rebars. From the trial and error tests, the embedded lengths were chosen to be 4 cm (1.57 in), 6 cm (2.36 in), and 8 cm (3.14 in). It is noted that the failure mode mainly depends on the quality of bond and the embedded length. The bond strength can be indirectly represented by the compressive strength of the concrete.

In the experimental set-up, no bond breakers were used to match the geometry given in the theoretical model. According to ASTM C-234-86 [13], for a given embedded length, three specimens were prepared. Data were obtained by taking the average of three specimens. The failure mode of the specimens was shear pull-out failure, and the error of each parameter required in the analysis, e.g., P_y, was within 7% of the average value for all the specimens.

Experimental Set-up

The pullout test procedure used in this study basically followed the specification of ASTM C-234-86 [13]. The bearing plate was designed to accommodate the specimens. The pullout test was performed in a universal material testing machine. The average value of two LVDT reading was used to control the stroke rate of 0.8 mm/min (0.0312 in/min). During the test, the loading and the displacement values were recorded using a data acquisition system. The displacement was measured at a position 4 cm (1.57 in) away from the surface of the concrete as shown in Figure 4. The effective displacement at point A was required for the analytical model. Thus, a desired U was computed as follows:

$$U_{desired} = U_{measured} - U_{offset} = U_{measured} - \frac{P * L_{off}}{E_f A}, \qquad (12)$$

where L_{off} is the offset length.

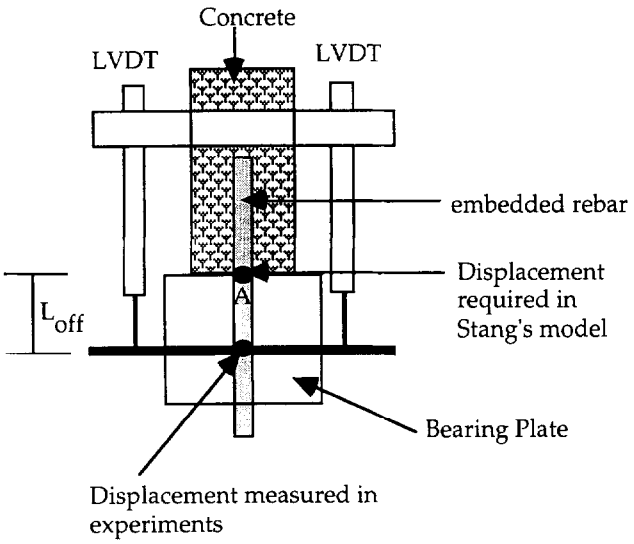

FIGURE 4. The offset length of the rebars.

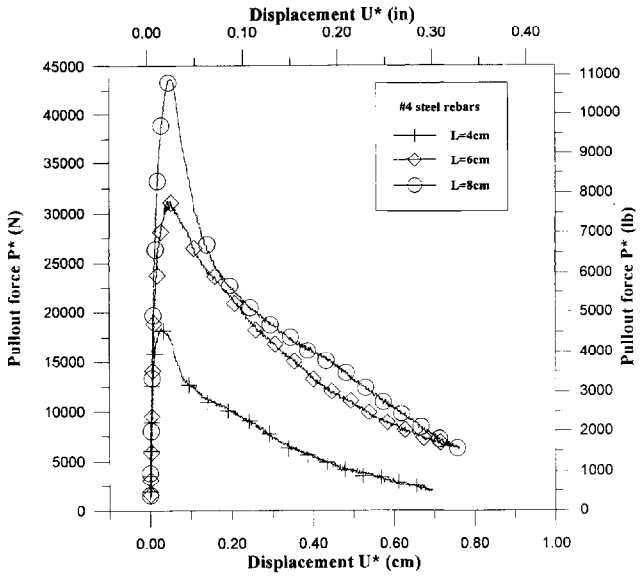

FIGURE 6. The pullout load-displacement curves for #4 rebars.

Experimental Results and Discussions

The experimental data for #3 and #4 steel rebars with various embedded lengths are given in Figures 5 and 6. The test results show that the initial linear slopes for different embedded lengths were almost the same for various rebars, and that the yield loading (P_y^*) and the maximum loading (P_{max}) were higher for the specimens with longer embedded lengths.

The four calculated parameters relating to interface properties are listed in Table 3. This table shows that the maximum loads and their corresponding displacement values for various embedded lengths agree with Stang's predictions. The value of D was independent of the embedded length and rebar size. The D value which represented the slip resistance after debonding was equal to 0.99, and this showed that the rebar-concrete interface still had strong interlock resistance after debonding. If the D value was set to be one, i.e., the elastic-perfectly plastic interface behavior model, the maximum load could still be predicted, however the surface energy, Γ, became zero in this proposed model, meaning another modification should be performed when calculating the strain energy in the shear lag and the work done by frictional forces. However, the D value was selected to be less than one. The Γ value obtained by using the displacement continuity approach was almost 100 times the value obtained by using the shear stress approach. As the Γ obtained by using the shear stress approach is too small compared with previous results, only the displacement continuity approach was chosen in the current research. Because the curve shape after debonding is mainly controlled by D when D is close to 1, the same curves were obtained using these two methods. It seems contradictory that the surface energy values Γ are different under different approaches, however, in the fracture mechanical approach, the surface energy is not a significant factor as long as the maximum load can be predicted precisely [18].

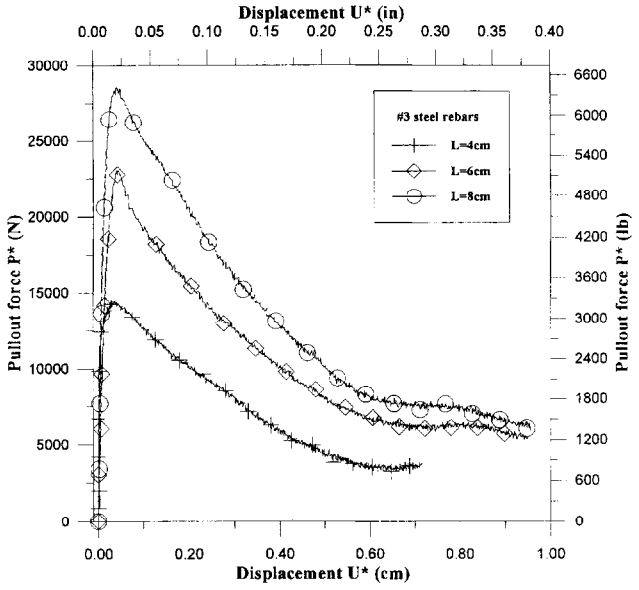

FIGURE 5. The pullout load-displacement curves for #3 rebars.

It was found that specimens with #4 rebar had higher surface energy values than did those with #3 rebar. The k values were different for specimens with #3 and #4 rebars, and it seems that specimens with #3 rebar had

TABLE 3. Parameters obtained from Stang's model

Parameters	Rebar #3			Number #4		
L cm (in)	4 (1.57)	6 (2.36)	8 (3.14)	4 (1.57)	6 (2.36)	8 (3.14)
P_y KN	13.24	19.42	22.56	17.66	27.96	36.30
(lbf)	(2976)	(4365)	(5070)	(3968)	(6283)	(8157)
k KN/cm^2	169.6	172.0	167.8	218.1	226.2	222.1
(kip/in^2)	(245.9)	(249.4)	(243.2)	(316.2)	(328.0)	(322.0)
k KN/cm^2		169.8			222.1	
(kip/in^2) average		(246.2)			(322.1)	
q_y KN/cm	3.522	3.702	3.508	4.619	5.158	5.371
(kip/in)	(2.011)	(2.113)	(2.002)	(2.637)	(2.944)	(3.066)
q_y KN/cm		3.577			5.049	
(kip/in) average		(2.042)			(2.882)	
P_{max}^{exp} KN	14.52	23.05	27.47	18.64	31.39	43.16
(kip)	(3.26)	(5.18)	(6.17)	(4.19)	(7.05)	(9.70)
$U_{P_{max}}^{exp}$ mm	0.24	0.27	0.30	0.24	0.28	0.33
(in)	(.0094)	(.011)	(.012)	(.0094)	(.011)	(.013)
The displacement continuity approach.						
$P_{max}^{(U)}$ KN	13.97	22.01	27.80	18.33	30.67	42.57
(kip)	(3.14)	(4.95)	(6.25)	(4.12)	(6.89)	(9.57)
$U_{P_{max}}^{(U)}$ mm	0.23	0.26	0.29	0.23	0.26	0.31
(in)	(.0091)	(.010)	(.011)	(.0091)	(.010)	(.012)
$\alpha_{P_{max}}^{(U)}$ mm	30.89	50.95	70.84	29.29	49.48	69.38
(in)	(1.216)	(2.006)	(2.789)	(1.153)	(1.948)	(2.731)
$D^{(U)}$	0.99	0.99	0.99	0.99	0.99	0.99
$D^{(U)}$ average		0.99			0.99	
$\Gamma^{(U)}$ N-m/m^2	12.21	13.30	12.24	12.25	14.72	16.26
(lbf-in/in^2)	(.0698)	(.0760)	(.0699)	(.0700)	(.0841)	(.0929)
$\Gamma^{(U)}$ N-m/m^2		12.58			14.41	
(lbf-in/in^2) average		(.0719)			(.0823)	

*Superscript (U) represents it is obtained from the displacement continuity approach, and superscript exp is the experimental result.

lower interface shear stiffness than did those with #4 rebar. The critical shear forces per length for debonding, q_y, were different for #3 and #4 rebars. It can be argued that q_y is not a true material parameter since it does not exclude the effect of the perimeter. If q_y were divided by the nominal perimeter of the rebar, the average critical shear stress was obtained and specimens with #4 rebar had higher values than did those with #3 rebar. This can be explained according to the geometry of rebars. The ratio of the rib height to the nominal diameter was 0.546 for #3 rebar and 0.661 for #4 rebar. This shows that the surface energy, the shear stiffness and the critical debonding stress were enhanced by additional rib interlock effect. Thus, a more complex model considering the geometry of deformed rebars should be developed to obtain the true material parameters. Nevertheless, such a theoretical model is not easy to derive, and the simplified model as mentioned in the analysis is acceptable in the engineering practical sense. If q_y values are divided by the nominal perimeter, the average interface yielding stresses 11.95 MPa (1,734 psi) and 12.77 MPa (1,835 psi) for #3 and #4 rebar-concrete interface can be obtained, respectively. Because the compressive strength was only about 35.9 MPa (5,200 psi), the estimated tensile strength of concrete was approximately at 3.59 MPa (520 psi). It seems contradictory that the failure mode should be splitting failure, not shear pull-out failure. The reason stems from the averaging of the rib's effect on the whole length. We propose a simplified estimation of the effective yielding shear stress as shown in Figure 7. Assume the effective yielding shear stress, τ_{eff}, acts on the surface of the rebar in one pitch, and that a normal force, N, acts on the inclined surface of the rebar where N is assumed to be related to Coulomb's frictional forces S, by $N = 1/\mu S$, in which μ represents the friction coefficient and S is obtained by integrating the shear stress on the inclined surface area of the rebar. From the equilibrium of the forces in the longitudinal direction, the following equation can be derived:

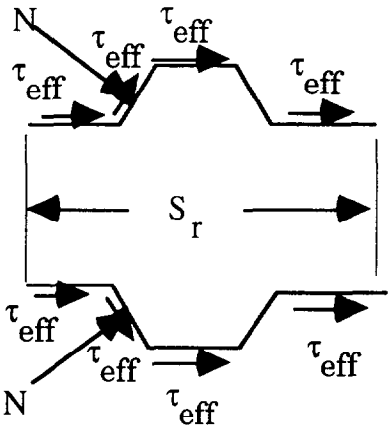

FIGURE 7. The simplified model for calculating τ_{eff}.

$$\frac{q_y S_r}{\pi} = \left[L_r(d_n + 2h_r) + (S_r - L_b)d_n + \frac{h_r^2 + h_r d_n}{\sin\beta}\left(\frac{\sin\beta}{\mu} + \cos B\right)\right]\frac{\tau_{eff}}{\sin\alpha}. \quad (13)$$

All the parameters in eq. 13 are defined in Table 2 or mentioned in the paragraph above. Substituting values from Table 2 and Table 3 into eq. 13 for specimens with #3 and #4 rebar, respectively. Then two equations for two unknown parameters, τ_{eff} and μ, can be obtained. Solving the two equations simultaneously, τ_{eff} is solved (3.94 MPa, 570 psi). The τ_{eff} value obtained in this approach is overestimated as the shear stress acting on the inner radius surface is higher than τ_{eff} when the shear stress acting on the outer radius surface is τ_{eff}. The indirect tensile strength test shows that to take 1/10 of the compressive strength as the estimated tensile strength might underestimate the tensile strength. Therefore, interface shear pullout failure may happen.

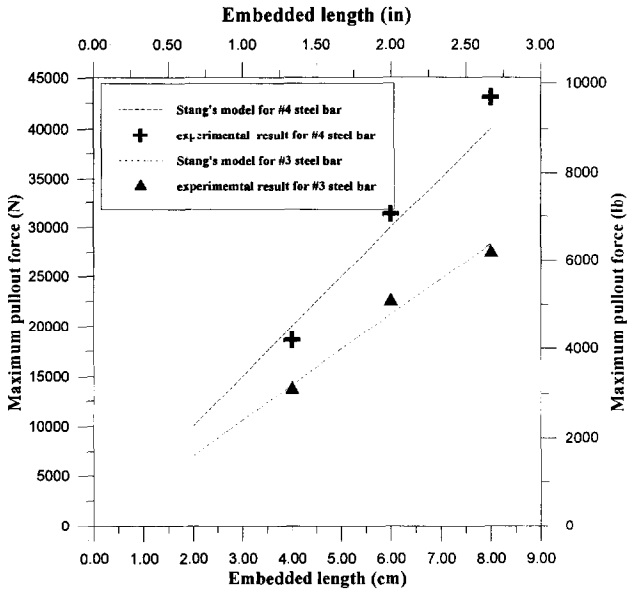

FIGURE 8. The comparisons of maximum pullout loading.

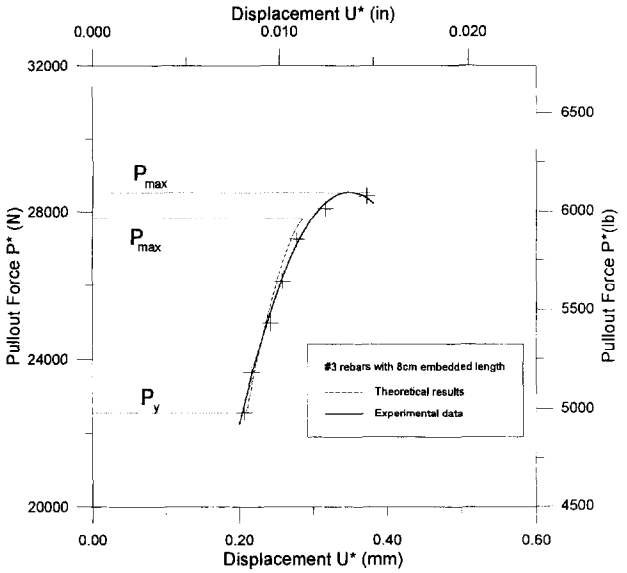

FIGURE 9. The deviations of Stang's model and experimental data.

Because the maximum load is the key factor as far as fracture mechanics is concerned, the maximum loads for different rebars and values from the theoretical model are compared in Figure 8. It is found that the theoretical results agree quite well with the experimental data.

The data obtained from experiments (for example, for the #3 rebars with 8 cm embedded length) are plotted and compared with the prediction curve in the second stage in Figure 9. It shows that displacement at the maximum pullout load obtained from the theoretical prediction is lower than that from the experiment. The difference results from the rigid matrix support assumption. In fact, the concrete surrounding the fiber is not a perfectly rigid support. If deformation of the concrete is considered, then the difference between the experimental data and theoretical results can be explained. However, the deviation is small and can be neglected.

Conclusions

Based on the test results and analysis, the theoretical model can be used to predict the interface properties of the rebar-concrete interface. The model derived originally for the cylindrical fiber can be adopted for deformed rebars with acceptable accuracy using the uniform distribution assumption. The predictions from the Stang's model fairly agree with the experimental results.

References

1. Najm, Naaman. *ACI Mat. J.*, **1991,** *88,* 2, 135–145.
2. Edwards, A.D.; Yannopoulos, P.T. *J. of ACI,* **1979,** Title No. 67–19, 405–420.
3. Soroushian *et al. ACI Mat. J.*, **1991,** *88,* 3, 227–232.
4. Ezeldin, A.S.; Balaguru, P.N. ***ACI Mat J.*, 1989,** *88,* 5, 515–524.
5. Hester, C.J. *et al. ACI Mat. J.*, **1993,** *90,* 1, 89–102.
6. Choi, O.C. *et al. ACI Mat. J.*, **1991,** *88,* 2, 207–217.
7. Ferguson, P.M. *et al. ACI J.*, **1962,** Proceedings *59,* 7, 887–992.
8. Orangun, C.O. *ACI J.* **1977,** 114–122.
9. Homayoun, H.A.; Mitchell, D. *ACI Mat. J.*, **1992,** *89,* 2, 161–167.
10. Maslehuddin, M. *et al. ACI Mat. J.*, **1990,** *87,* 5, 497–502.
11. Bažant, Z.P.; Sener, S. *ACI Mat. J.*, **1988,** *85,* 5, 347–351.
12. Balazs, G.L. *ACI Mat. J.*, **1993,** *90,* 4, 340–348.
13. Hamoush, S.A.; Salami, M.R. *ACI Str. J.*, **1990,** *87,* 6, 678–686.
14. Stang, H. *et al. ASCE J. Eng. Mech.*, **1990,** *116,* 10, 2136–2149.
15. Reinhardt, H.W. *et al. Materiaux et Constructions,* **1984,** *17,* 100, 311–320.
16. Ezeldin, A.S.; Balaguru, P.N. *Computers & Structures,* **1990,** *37,* 4, 569–584.
17. ASTM C234-86. *Standard test method for comparing concretes on basis of the bond developed with reinforced steel. ASTM annual book of standards, section 4, construction,* **1988.**
18. Broek, D. *The Practical Use of Fracture Mechanics,* Kluwer Academic Publishers, **1988.**